esa ECOSPHERE

Wildfire impacts on forest microclimate vary with biophysical context

KYRA D. WOLF [1,†] PHILIP E. HIGUERA [1] KIMBERLEY T. DAVIS [1] AND SOLOMON Z. DOBROWSKI [2]

[1]*Department of Ecosystem and Conservation Sciences, University of Montana, 32 Campus Drive, Missoula, Montana 59812 USA*
[2]*Department of Forest Management, University of Montana, 32 Campus Drive, Missoula, Montana 59812 USA*

Citation: Wolf, K. D., P. E. Higuera, K. T. Davis, and S. Z. Dobrowski. 2021. Wildfire impacts on forest microclimate vary with biophysical context. Ecosphere 12(5):e03467. 10.1002/ecs2.3467

Abstract. Increasing wildfire activity in western North America has the potential to remove forest canopy cover over large areas, increasing the vulnerability of understory plants and juvenile trees to microclimatic extremes. To understand the impacts of wildfire on forest microclimatic buffering, we monitored daily temperature and vapor pressure deficit (VPD) in 33 plots over the first two growing seasons following two wildfires from 2017. The Lolo Peak and Sunrise fires occurred during a regionally extensive fire season, burning mixed-conifer and subalpine forests across complex mountainous topography in western Montana. Sensors were deployed from June to September in 2018 and 2019 in sites stratified by aspect, elevation, and fire severity (unburned, moderate, high) to capture a range of forest types, biophysical contexts, and fire effects. Loss of canopy and understory vegetation had marked effects on microclimate: On average, sites burned at high severity had 3.7°C higher daily maximum temperatures and 0.81 kPa higher daily maximum VPD relative to paired unburned sites. Differences between burned and unburned sites were most pronounced when ambient temperatures were high, across diurnal and seasonal time scales. Differences were also more pronounced at sites with less canopy cover, more bare ground postfire, and greater long-term water availability (i.e., low climatic water deficit). Our results reveal fire-caused changes in microclimate extremes that are biologically meaningful for the postfire establishment of tree seedlings and understory vegetation. These effects depend strongly on biophysical context, with cool-wet forests more vulnerable to fire-caused changes in microclimate compared with warm-dry settings. Our results further highlight the functional importance of standing dead trees for moderating surface temperature in postfire environments. Anticipating forest ecosystem responses to increased warming and wildfire activity, and the potential for fire to catalyze vegetation changes, thus requires considering the substantial impacts of fire on microclimate.

Key words: biophysical gradient; conifer forest; fire severity; microclimate; microclimatic buffering; Rocky Mountains; wildfire.

Received 14 May 2020; accepted 7 December 2020; final version received 26 January 2021. Corresponding Editor: Carrie R. Levine.

† **E-mail** : Kyra.Wolf@umontana.edu

INTRODUCTION

Wildfire is a longstanding natural disturbance in forest ecosystems of western North America, where increased aridity in recent decades is well linked to increased area burned and fire severity (Gillett et al. 2004, Westerling 2016, Abatzoglou and Williams 2016, Holden et al. 2018, Parks and Abatzoglou 2020). Such trends are expected to continue in upcoming decades under warmer and drier conditions (Flannigan et al. 2005, Westerling et al. 2011, McKenzie and Littell 2017, Young et al. 2017) and, combined with increasingly stressful conditions for tree regeneration,

are expected to lead to widespread vegetation change (Anderson-Teixeira et al. 2013, Serra-Diaz et al. 2018, Coop et al. 2020). While wildfire plays an important role in stimulating tree regeneration and understory growth by increasing the availability of light, nutrients, and mineral seedbeds (e.g., Hesketh et al. 2009, Ma et al. 2010, Crotteau et al. 2013, Brown et al. 2015), fire-caused tree mortality also alters microclimate conditions. Given that tree seedlings are sensitive to climatic stressors (Johnson et al. 2011, Andrus et al. 2018, Davis et al. 2018, 2019*a*, Kemp et al. 2019), fire-induced changes in microclimate are a likely mechanism through which warming and increased wildfire activity will impact forest ecosystems.

Wildfires can alter understory microclimates through several mechanisms, perhaps most importantly by reducing canopy cover. Relative to areas with no tree canopy, environments under forest canopies experience smaller variations between maximum and minimum temperatures due to reduced direct insolation and longwave emission, with more pronounced differences as canopy cover increases (Montes-Helu et al. 2009, Suggitt et al. 2011, von Arx et al. 2013, Frey et al. 2016, De Frenne et al. 2019, Davis et al. 2019*b*). Microclimatic buffering also varies spatially and temporally with macroclimate. Buffering is more pronounced in forests with greater local water availability to support evaporative cooling (Davis et al. 2019*b*), and buffering is often more pronounced when ambient conditions are warmer and drier (von Arx et al. 2013). Thus, based on canopy loss alone, recently burned areas are expected to experience greater temperature extremes relative to unburned forests, with larger changes in areas of greater canopy loss (Ma et al. 2010) and in forests with greater prefire evaporative cooling.

Wildfires do more than simply reduce canopy cover, however, and the potential impacts of these changes in microclimatic buffering have received relatively little attention (Ma et al. 2010, Brown et al. 2014, Refsland and Fraterrigo 2018). Recently burned areas comprise a mosaic of varying fire effects, including tree mortality and impacts on understory cover, which in turn affect the degree to which shading, surface roughness, evapotranspiration, and albedo are altered relative to unburned forest (Liu 2005, Chambers 2005, Liu et al. 2019). For example, structural features such as standing dead trees may lessen the impacts of canopy loss on microclimate in burned areas (Hoecker et al. 2020), and changes in surface cover after fire affect land surface temperatures (Liu et al. 2019). Anticipating the vulnerability of forest vegetation to the combined effects of changing climate and fire regimes thus requires understanding the impacts of wildfires on microclimatic buffering, and the degree to which these impacts vary across fire severity and biophysical gradients.

To understand how fire severity and biophysical context interact to influence microclimate conditions relevant to plant regeneration, we monitored near-ground air temperature and vapor pressure deficit (VPD) over the first two growing seasons after two wildfires in the U.S. northern Rocky Mountains. We sampled 33 sites, 11 of which were unburned, spanning gradients in fire severity, local water balance, and forest type. We focused on areas that burned at moderate or high severity, where postfire tree regeneration is most critical for forest resilience to wildfire, and where microclimate is most likely to be influenced by fire-induced changes in forest canopy and understory cover. We expected that recently burned forests would experience greater microclimate extremes relative to unburned forests, with effects scaling directly with fire severity due to greater canopy loss, reduction in evapotranspiration, and initial decreases in surface albedo. We further expected that the relative effect of wildfire on microclimate would vary across time and space, with greater effects during times when ambient temperatures were high (e.g., hours within a day and days within a season), and in more mesic sites where high evapotranspiration leads to greater microclimatic buffering capacity (von Arx et al. 2013, Davis et al. 2019*b*).

Methods

Study area and site selection

The study was conducted in the Lolo National Forest, in the northern Bitterroot Mountains of Montana (Fig. 1). The region is characterized by complex mountainous topography, with vegetation composition varying with elevation, slope, and aspect. At low to

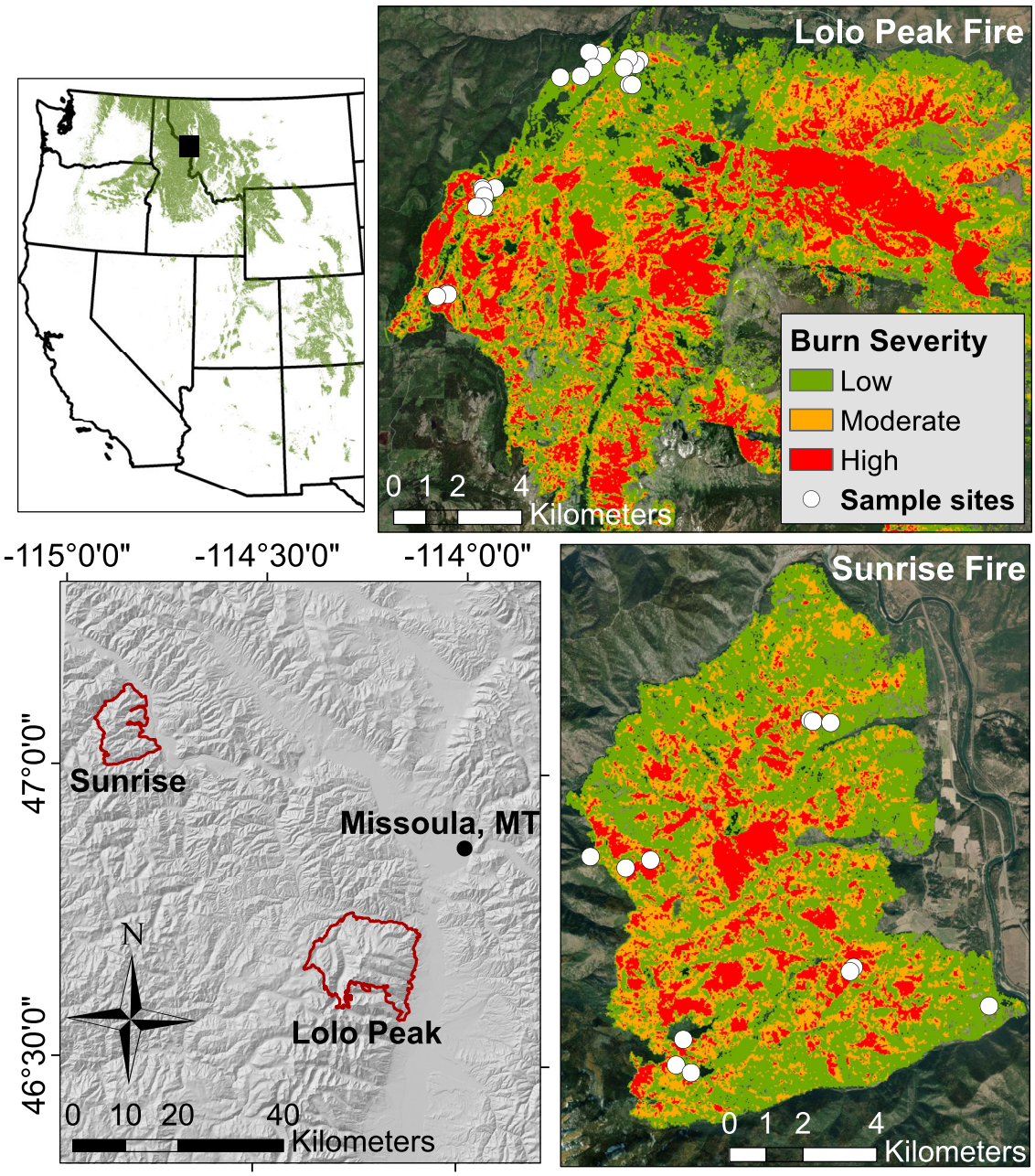

Fig. 1. Map of sampling locations in the 2017 Sunrise (n = 12) and Lolo Peak (n = 21) fires, showing fire severity classifications obtained from the Monitoring Trends in Burn Severity program (MTBS). Inset shows the location of study area (black square), with the green shaded area indicating the extent of Rocky Mountain mixed-conifer and subalpine forest classes mapped by the LANDFIRE program (landfire.gov).

mid-elevations (i.e., <1500 m) and xeric aspects, ponderosa pine (*Pinus ponderosa*), Douglas fir (*Pseudotsuga menziesii*), and western larch (*Larix occidentalis*) typically dominate. Subalpine forest extends from ~1500 to 2200 m in elevation, with dominant species including lodgepole pine (*Pinus contorta* var. *latifolia*), subalpine fir (*Abies lasiocarpa*), and Engelmann spruce (*Picea*

engelmannii). In the northern end of the study area, mountain hemlock (*Tsuga mertensiana*) is also present at high elevations. Common understory species include green alder (*Alnus viridis*) and common huckleberry (*Vaccinium globulare*), with fireweed (*Epilobium angustifolium*) typically present in recently burned areas. Averaged across sites for the period 1981–2010, mean annual temperature is 5.2°C and annual precipitation is 987 mm, with 20% falling during the snow-free season from June to September (PRISM C*limate* G*roup*).

We sampled 33 plots within two large fires that burned from July to September 2017, a regionally extensive fire year associated with above-average warmth and aridity (Balch et al. 2018; Fig. 1). The Lolo Peak Fire affected ~22,000 ha, with 20% of the fire area classified as high severity, 20% as moderate severity, 37% as low severity, and 23% as unburned (MTBS). The Sunrise Fire affected ~11,000 ha, with 15% high severity, 28% moderate severity, 53% low severity, and 4% unburned (MTBS). Potential study areas within each fire were identified using USFS Burned Area Reflectance Classification soil burn severity maps (30-m resolution), which are based on satellite imagery with field verification by emergency response teams, and are available prior to publication of MTBS burn severity products (fsapps.nwcg.gov). To achieve the goal of sampling across biophysical gradients, sites were stratified by elevation (low, 1000–1500 m, and high, 1500–2000 m) and aspect (northern, 315°–45°, and southern, 135°–225°). Within each stratum, we sampled an unburned plot, a plot that burned at high severity, and a plot that burned at moderate severity; each unburned plot was used as a reference for the two burned plots in the same stratum. This yielded 11 plots each in the unburned, moderate-, and high-severity categories. The median distance between paired burned and unburned sites was 0.48 km (Appendix S1: Table S1). Exact sampling locations were randomly identified in a geographic information system to satisfy these criteria and avoid planned salvage logging (K. Wetzstein, *personal communication*), while also being within 2 km of a road to ensure accessibility. Precise plot locations were shifted in the field where necessary to sample in the targeted severity class, based on a visual assessment of tree mortality and, for unburned plots, the absence of charred surface fuels and trees. Of the 33 plots, seven were moved up to 100 m from their original locations, and one unburned plot was moved 2 km.

Field measurements and data aggregation

Plot characteristics were measured using a 60-m long belt transect parallel to the fall line, which in most cases extended upslope from a microclimate sensor post (described below). Within each transect, overstory tree density, species composition, and percent mortality were quantified, and live and dead basal area was measured at meter 0, 30, and 60 on the transect. At 6–10 evenly spaced points along each transect, live and dead canopy cover was measured using a spherical densiometer, the distance to the nearest live tree was measured using a laser range finder, and bole scorch height of the nearest tree was measured as a coarse metric of fire behavior. At each of these points, ground cover measurements were taken using a 1-m^2 quadrat to quantify percent cover of bare ground or rock, litter, and vegetation. Plot averages of each metric were calculated. In addition, canopy cover at the location of the sensor post was measured and recorded separately as the sensor-specific canopy cover.

At each plot, a sensor measuring temperature and relative humidity was attached to a metal conduit pole 10 cm above the ground surface, within a radiation shield that performs similarly to commercially available shields (Holden et al. 2013). In 2018, data were collected from a total of 15 plots (five in each severity class) in the Lolo Peak Fire to capture the first postfire growing season. In 2019, microclimate was monitored again at six of these original plots in the Lolo Peak Fire. In addition, 18 new plots were sampled in 2019: six in the Lolo Peak Fire and 12 in the Sunrise Fire. This yielded a sample size of 33 plots across both fires and years (Appendix S1: Table S1).

Sensors recorded temperature (T, °C) and relative humidity (RH, %) on half-hourly time steps over the snow-free season (June–September). Appendix S1 describes sensor calibration, used to account for the use of two different sensor models over the study, as well as quality control procedures. Vapor pressure deficit (VPD, kPa) was calculated based on temperature and

relative humidity, using the following equation (cf. Monteith and Unsworth 2013):

$$\mathrm{VPD} = \left[0.6112 \times e^{\frac{17.62 \times T}{T+243.12}}\right] \times \mathrm{RH}/100.$$

Data for each plot were aggregated to daily maximum temperature and daily maximum VPD by selecting the highest value over each 24-h calendar day, regardless of the time at which it occurred (Appendix S1). The difference in daily maximum temperature and VPD between each burned site and its paired unburned site was then calculated ($\Delta T_{\max}$, $\Delta V_{\max}$) and used as a response variable in further analyses. We focused on daily maxima because these represent stressful conditions for plants, and we used $\Delta T_{\max}$ and $\Delta V_{\max}$ as a metric of fire-caused change in warm-dry microclimatic extremes.

Site-level metrics of fire severity

We used both categorical (satellite-derived) and continuous (field-based) metrics of fire severity in our analyses. First, we used the plot-averaged dNBR metric from the Monitoring Trends in Burn Severity program (released after site selection in 2018) to classify plots into discrete fire severity classes. We report nonparametric statistical comparisons of microclimate conditions among these discrete classes using Wilcoxon rank-sum tests. Second, we characterized fire severity at each plot using a suite of field measurements reflecting fire effects more precisely than satellite-derived metrics alone. We summarized these measurements using a PCA, described in detail in Appendix S1. We used the first two principal components as predictor variables in our statistical models, allowing us to quantify distinct aspects of fire severity that do not covary. PCA Axis 1 (hereafter Axis1) reflects plot-averaged live canopy cover and basal area (positive values), and dead canopy cover and basal area, tree mortality, scorch height, and distance to seed source (negative values). PCA Axis 2 (hereafter Axis2) primarily reflects ground cover, with positive values associated with greater bare ground cover and negative values associated with greater vegetation cover; in burned plots, these values represent understory regrowth after fire. We thus interpret Axis1 as a metric of overstory fire effects and Axis2 as a metric of understory fire effects, and refer to these metrics as "field-based fire severity."

Macroclimate gradients

To characterize the biophysical context of each plot, we calculated the long-term climatic water deficit (DEF, mm) by averaging annual values from 1981 to 2015 from a 250-m resolution downscaled climate product described by Holden et al. (2016, 2018). DEF thus represents a time-integrated measure of local water balance. We also calculated the heat load index (HLI) at 1/3 arc-second (~10 m) resolution following the McCune and Keon (2002) method using the spatialEco package in R. HLI is a unitless index that integrates the effects of aspect, slope, and latitude on potential solar heating. HLI and DEF were not significantly correlated ($r = 0.28$; $P = 0.21$, $t = 1.3$, df = 20).

To characterize temporal variability in ambient climate conditions at each plot, we used daily maximum temperature over the 2018 and 2019 sampling periods from the 4-km resolution gridMet product (Abatzoglou 2013). Study plots spanned seven distinct grid cells, with all but three sets of paired plots falling within a single grid cell. We used the gridMet-based temperature as a proxy for daily ambient (free-air) conditions at each plot ($T_{\max}A$, °C). This is well-justified, given that gridMet-derived daily temperatures were significantly correlated with sensor-measured daily temperature maxima at each plot, with an average correlation coefficient of 0.95 across all plots ($P < 0.0001$, $t = 34$, df = 100).

Statistical analyses

We used linear mixed-effects models to quantify the relative influence of field-based fire severity, biophysical site characteristics, and ambient weather conditions on daily differences in maximum temperature and VPD between burned and unburned sites ($\Delta T_{\max}$ and $\Delta V_{\max}$). To minimize the effects of temporal autocorrelation, we subsampled each time series to retain one day out of every eight consecutive days, for a total of 29 d of observations (i.e., 13 d in 2018 and 16 d in 2019). This subsetting procedure was selected because a preliminary analysis of temporal autocorrelation at each site indicated significant autocorrelation for up to seven to eight days. Random intercept terms for the effects of site and sampling year (nested within site) were included to account for repeated measurements from the

same sites within and between years. Predictor variables included site characteristics describing fire severity (Axis1 and Axis2) and biophysical context (DEF and HLI), as well as daily ambient weather conditions ($T_{max}A$; Table 1). We also considered three additional predictor variables to account for biophysical differences between paired burned and unburned plots (Table 1). These were the difference in HLI and DEF between each paired burned and unburned plot, ΔHLI and ΔDEF, and the difference in canopy cover above the sensor post, ΔCanopy. While values of ΔHLI and ΔDEF were generally small due to our stratified sampling design, ΔCanopy varied among sites and was retained in the reduced models. Alternate modeling approaches yielded similar results (e.g., directly modeling maximum temperature or VPD of the burned plots as a function of measured conditions in the unburned plots).

To evaluate the relative influence of canopy cover, topography, and fire severity on microclimate, we conducted model selection with different subsets of predictor variables and compared among the resulting subset models. A simple null model assumed that ΔT_{max} and ΔV_{max} were a function of ambient temperature ($T_{max}A$) and the difference in canopy cover between the burned and unburned plot (ΔCanopy). The "topo" subset model added variables describing the biophysical context (DEF and HLI) to the null model, based on the hypothesis that topography mediates the effect of canopy loss on microclimate. The "fire" subset model added variables describing fire severity (Axis1 and Axis2) to the null model, based on the hypothesis that canopy loss and other fire effects (e.g., tree mortality, understory change) influence microclimate conditions. The full "topo + fire" model considered all predictors noted above. All models considered a quadratic term for $T_{max}A$ and interaction terms (up to two-way) among predictors (e.g., $T_{max}A$, HLI, DEF, Axis1, and Axis2).

We conducted model selection for each subset model described above and used cross-validated root-mean-square error (RMSE) to evaluate model skill, ultimately selecting a single final model each for temperature and VPD (Table 2).

Table 1. Description of the response and predictor variables used in the statistical models.

Variable name	Code	Units	Description
Response variables			
Daily difference in maximum temperature	ΔT_{max}	°C	Difference in daily maximum temperature between paired burned and unburned sites
Daily difference in maximum VPD	ΔV_{max}	kPa	Difference in daily maximum vapor pressure deficit between paired burned and unburned sites
Explanatory variables			
Ambient conditions			
GridMET daily maximum temperature	$T_{max}A$	°C	Daily maximum temperature derived from gridMET (4-km resolution; Abatzoglou 2013)
Biophysical site characteristics			
Climatic water deficit	DEF	cm	Mean annual climatic water deficit, a measure of unmet atmospheric demand for water, averaged over 1981–2015 for each burned site (250-m resolution)
Heat load index	HLI	Unitless	Index of potential solar heating based on slope, aspect, and latitude of each burned site (~10-m resolution)
Field-based fire severity			
PCA Axis 1	Axis1	Unitless	Index of fire severity based on plot-averaged tree mortality and live and dead canopy cover, derived from PCA (Appendix S1: Fig. S3)
PCA Axis 2	Axis2	Unitless	Index of fire severity and vegetation regrowth based on plot-averaged ground cover, derived from PCA (Appendix S1: Fig. S3)
Site-difference variables			
Difference in canopy cover from unburned	ΔCanopy	%	Difference in total canopy cover directly over the sensor post between burned and unburned plots
Difference in DEF	ΔDEF	mm	Difference in climatic water deficit between burned and unburned plots
Difference in HLI	ΔHLI	Unitless	Difference in heat load index between burned and unburned plots

Models were selected initially through backward elimination to retain all significant terms based on *F*-tests ($P < 0.05$) using the lmerTest package in R (Kuznetsova et al. 2017). To avoid overfitting the data, we considered dropping additional terms based on cross-validated RMSE. We used a leave-one-out cross-validation procedure by holding out the data from one plot and training the model on the data from the remaining 21 plots, and then predicting on the holdout data and calculating the RMSE; this was repeated for all plots to obtain an average cross-validated RMSE. In selecting the final models for ΔT_{max} and ΔV_{max}, we balanced predictive skill (RMSE) with parsimony.

Results

Daily differences in maximum temperature (ΔT_{max}) and VPD (ΔV_{max}) between paired burned and unburned plots varied throughout the season, with the largest differences occurring when daily temperatures were highest (Appendix S2: Fig. S1). Averaged across the season, daily maximum temperatures were 3.7 ± 2.4°C (standard deviation) higher in sites classified as high severity relative to unburned sites ($P = 0.015$, $W = 82$, $n = 11$). Across both severity classes, maximum temperatures were 2.6 ± 2.7°C higher on average in burned sites than in unburned sites ($P = 0.048$, $W = 338$, $n = 22$; Fig. 2). Maximum daily VPD was 0.81 ± 0.40 kPa (58%) higher on average in sites burned at high severity than in unburned sites ($P = 0.003$, $W = 107$, $n = 11$), and 0.52 ± 0.54 kPa (30%) higher in burned than unburned sites across both fire severity classes ($P = 0.024$, $W = 180$, $n = 22$). Average daily minimum temperature and VPD were not significantly different in burned compared with unburned sites (*P* values > 0.10; Fig. 2).

When predicting ΔT_{max}, the model including topography and fire severity (topo + fire model) provided the best predictive skill, with an average cross-validated RMSE of 2.50 ± 0.90°C (SD; Table 2). Differences in daily maximum temperatures (ΔT_{max}) were explained by canopy cover (ΔCanopy), ambient weather conditions ($T_{max}A$), long-term climatic water deficit (DEF), ground cover (Axis2), potential solar heating (HLI), and interaction terms among these variables (Appendix S2: Table S1). Burned and unburned sites with greater differences in canopy cover above the sensor tended to have larger differences in daily maximum temperatures (Fig. 3). Values of ΔCanopy were not significantly correlated with Axis1 values ($r = 0.27$; $P = 0.23$, $t = 1.2$, df = 20) or dNBR ($r = -0.11$; $P = 0.63$, $t = -0.48$, df =

Table 2. Comparison among candidate models, showing terms retained in final models and average cross-validated RMSE (± 1 SD).

Model	Predictors considered	Fixed-effects terms	RMSE†
Temperature (ΔT_{max})			
Null	ΔCanopy, $T_{max}A$	ΔCanopy + $T_{max}A$	2.82 ± 1.23
Topo	ΔCanopy, $T_{max}A$, DEF, HLI	ΔCanopy + $T_{max}A$ + DEF + $T_{max}A$:DEF	2.80 ± 0.96
Fire	ΔCanopy, $T_{max}A$, Axis1, Axis2	ΔCanopy + $T_{max}A$ + Axis2 + $T_{max}A$:Axis2	2.75 ± 1.01
Topo + Fire‡	ΔCanopy, $T_{max}A$, DEF, HLI, Axis1, Axis2	ΔCanopy + $T_{max}A$ + DEF + Axis2 + HLI + $T_{max}A$:DEF + HLI:DEF + HLI:Axis2	2.50 ± 0.90
VPD (ΔV_{max})			
Null	ΔCanopy, $T_{max}A$	ΔCanopy + $T_{max}A$ + $T_{max}A^2$	0.67 ± 0.36
Topo‡	ΔCanopy, $T_{max}A$, DEF, HLI	ΔCanopy + $T_{max}A$ + $T_{max}A^2$ + DEF + $T_{max}A$:DEF + $T_{max}A^2$:DEF	0.62 ± 0.25
Fire	ΔCanopy, $T_{max}A$, Axis1, Axis2	ΔCanopy + $T_{max}A$ + $T_{max}A^2$ + Axis2 + $T_{max}A$:Axis2 + $T_{max}A^2$:Axis2	0.65 ± 0.32
Topo + Fire	ΔCanopy, $T_{max}A$, DEF, HLI, Axis1, Axis2	ΔCanopy + $T_{max}A$ + $T_{max}A^2$ + DEF + Axis2 + HLI + $T_{max}A$:DEF + $T_{max}A^2$: DEF + HLI:DEF + HLI:Axis2	0.60 ± 0.31

Notes: Models include a null model (canopy cover only), a topo model (canopy cover + topographic variables), a fire model (canopy cover + fire severity variables), and a topo + fire model considering all potential predictors. Variable codes are described in Table 1.

† Values for RMSE for ΔT_{max} are in °C and that for ΔV_{max} are in kPa.

‡ Indicates selection as the final model reported on in the text.

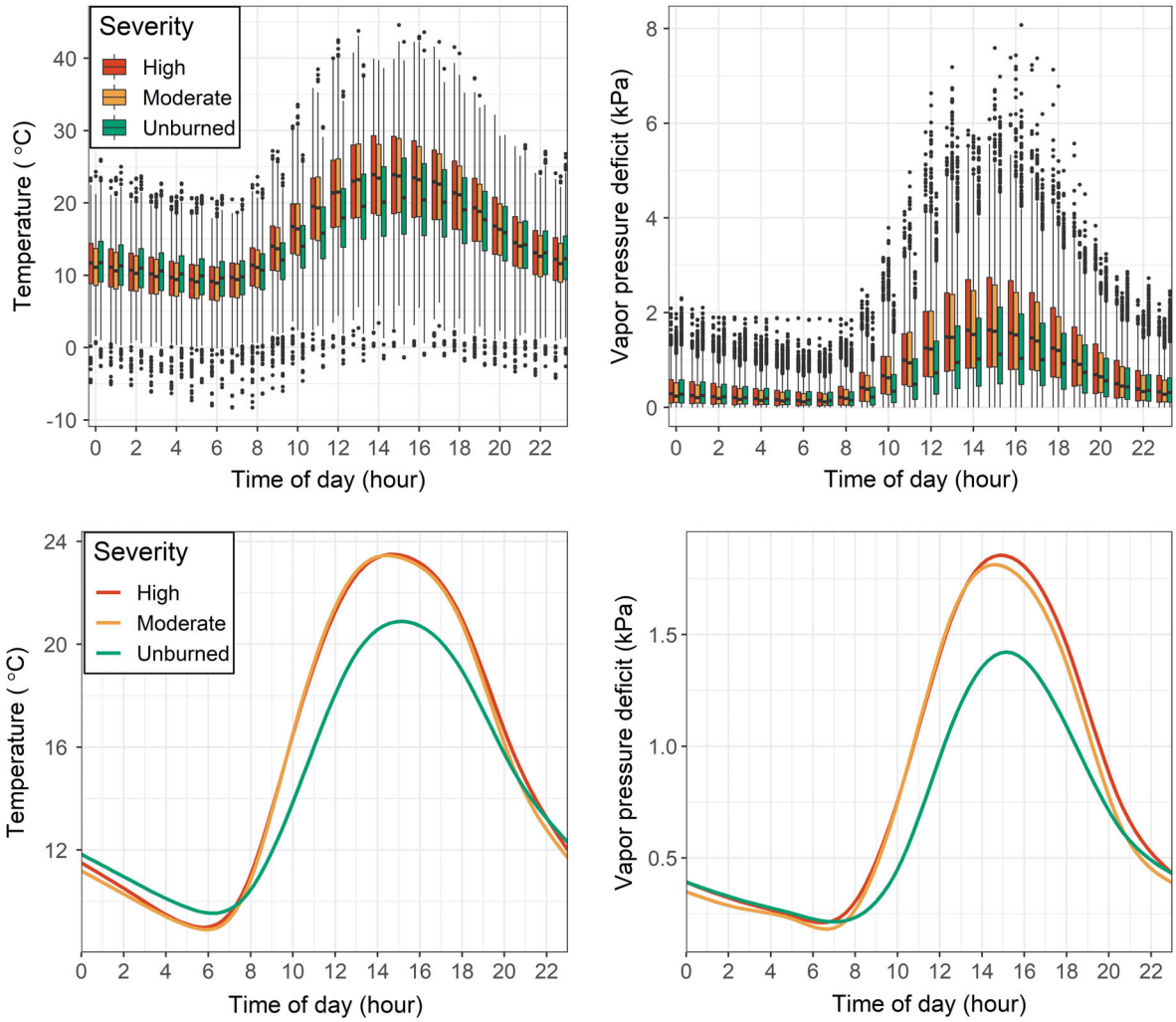

Fig. 2. Diurnal variability in VPD (kPa) and temperature (°C) across all sensors and years, aggregated to hourly time steps and displayed using boxplots (top panel) and curves fit by time of day using generalized additive models (mgcv package in R; bottom panel). Sensors are grouped by fire severity classifications (high, moderate, unburned) based on field measurements.

20), suggesting that this effect of canopy cover is not reflected in field-based fire severity metrics at the plot scale.

After accounting for differences in canopy cover, ΔT_{max} generally increased with $T_{max}A$, but the effect was contingent on DEF. Differences in daily maximum temperatures (ΔT_{max}) tended to be low in sites with high DEF (i.e., warm-dry sites) and varied little with ambient temperatures ($T_{max}A$; Fig. 4); in contrast, ΔT_{max} increased with $T_{max}A$ in sites with low DEF (i.e., cool-moist sites). For example, on days when ambient temperatures were high (i.e., exceeding the 75th percentile of 26.7°C), ΔT_{max} averaged 6.1 ± 2.1°C among sites with low DEF (i.e., below the 25th percentile) and -0.02 ± 3.1°C among sites with high DEF (i.e., above the 75th percentile). In addition, ΔT_{max} was lower in sites with above-average HLI (i.e., above the 50th percentile), averaging 1.6 ± 2.1°C; this contrasts with an average ΔT_{max} of 2.6°C across all sites. This effect was contingent on both DEF and Axis2. Differences in maximum temperatures (ΔT_{max}) tended to be low in warm, dry sites with

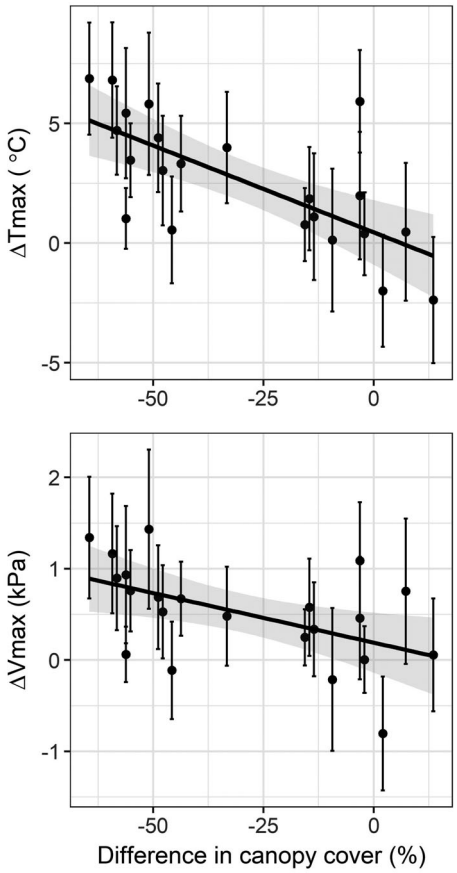

Fig. 3. Bivariate relationship between the difference in canopy cover above the sensor in paired burned and unburned plots (ΔCanopy, *x*-axis) and ΔT_{max} (top panel), and ΔV_{max} (bottom panel). Positive ΔT_{max} and ΔV_{max} values indicate warmer/drier conditions in the burned plot than the unburned plot, and negative ΔCanopy values indicate less canopy cover in the burned plot than the unburned plot. Plot averages ±2 SEs are shown, as well as a simple linear fit with 95% confidence intervals (shaded bands).

high HLI and DEF, but varied little with HLI among sites with low DEF or high vegetation cover (i.e., negative Axis2 values; Fig. 4). Further, ΔT_{max} tended to be greater in sites with more exposed ground (i.e., above the 75th percentile of Axis2 values), averaging 4.4 ± 2.2°C, with smaller ΔT_{max} among sites with high HLI (Fig. 4). Overall, ΔT_{max} depended on canopy cover, ambient weather conditions, biophysical context, and fire severity.

When predicting ΔV_{max}, the model including topography only (topo model) had the best combination of predictive skill and parsimony, with an average cross-validated RMSE of 0.62 kPa ± 0.25 (SD; Table 2). Differences in daily maximum VPD (ΔV_{max}) were explained by ΔCanopy, $T_{max}A$, DEF, a quadratic term of $T_{max}A$, and an interaction term between $T_{max}A$ and DEF (Appendix S2: Table S1). Average ΔV_{max} was greater in sites with larger differences in canopy cover (Fig. 3). After accounting for this effect, ΔV_{max} tended to increase at higher ambient temperatures ($T_{max}A$), but the effect was contingent on DEF, exhibiting a pattern similar to the model for ΔT_{max} described above. Cooler, moister sites (i.e., low DEF) had a strong positive relationship between ΔV_{max} and $T_{max}A$, whereas warmer, drier sites (i.e., high DEF) had less variation in ΔV_{max} (Fig. 5). For example, on days when ambient temperatures were high (i.e., exceeding the 75th percentile), ΔV_{max} averaged 1.55 ± 0.56 kPa at sites with low DEF (i.e., below the 25th percentile) and −0.22 ± 0.90 kPa at sites with relatively high DEF (i.e., above the 75th percentile). The topographic variable representing potential solar exposure (HLI) was not retained in the final model, perhaps because the effect of topography on local climate is, to some degree, reflected in the calculation of climatic water deficit, although at a different spatial resolution. Overall, ΔV_{max} depended on canopy cover, ambient weather conditions, and local water balance.

Discussion

Our study documents substantial impacts of wildfire on microclimatic extremes in forest ecosystems, quantifying changes that are biologically meaningful for the postfire reestablishment of tree seedlings and understory vegetation. We also highlight that these impacts vary significantly based not only on ambient conditions and fire severity, but also on the biophysical context of a site, including long-term climatic water deficit. Our findings thus have important implications for anticipating forest ecosystem responses to increasing moisture deficits and fire activity expected in the future, and they provide quantitative information useful in modeling such scenarios.

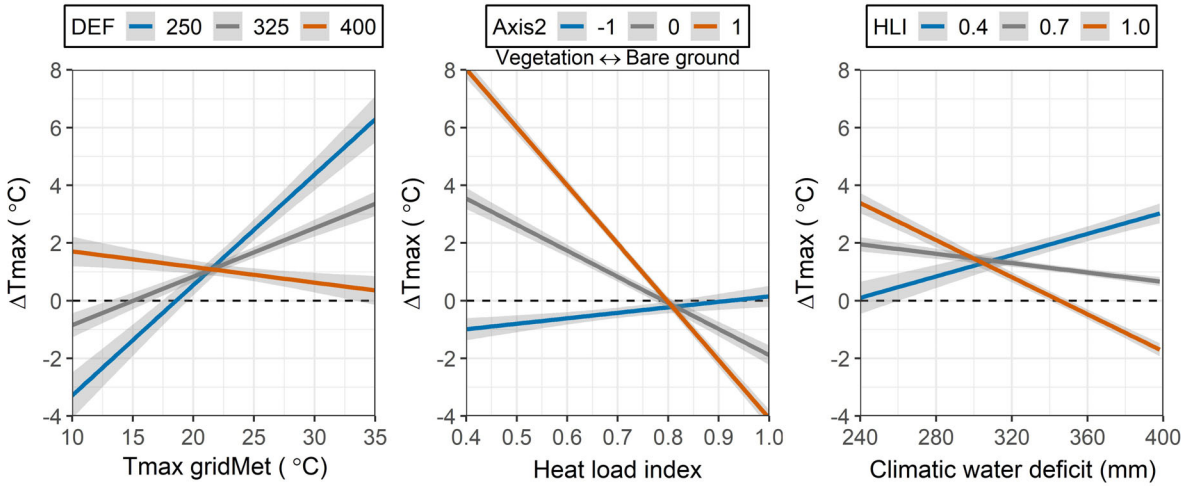

Fig. 4. Model predictions of ΔT_{max} after controlling for differences in canopy cover between paired burned and unburned sites, where positive ΔT_{max} values indicate higher temperatures in the burned plot. Trends in ΔT_{max} are graphed to show the effects of interaction terms among ambient weather ($T_{max}A$), mean annual climatic water deficit (DEF, mm), heat load index (HLI), and Axis2 (left panel to right panel). High DEF indicates lower long-term moisture availability. Negative Axis2 values indicate greater understory vegetation cover, while positive values indicate greater bare ground cover. High HLI indicates higher potential solar heating. Shaded bands show 95% confidence intervals for linear fits.

Fire-related changes in microclimate are biologically meaningful

Our results indicate that warm, dry microclimatic extremes near the ground surface are amplified in the postfire environment relative to unburned forest stands, with the strongest effects occurring when ambient temperatures are highest (Fig. 2; Appendix S2: Fig. S1). These effects are likely due to increased surface radiation intensity, reduced evaporative cooling, and increased sensible heating in the postfire environment. The buffering effects of canopies are largely a function of light interception and evaporative cooling through transpiration (von Arx et al. 2013, Davis et al. 2019*b*). Initially after a fire, reduced light interception and reduced albedo due to charring and loss of plant cover increase surface radiation intensity during the snow-free season, which contributes to higher surface temperatures and greater potential for heating of soil and air (Ripley and Archibold 1999, Chambers 2005, Tsuyuzaki et al. 2009, Ma et al. 2010, Liu et al. 2019). Further, reduced evapotranspiration decreases latent heat flux and increases sensible heating in recently burned forests (Liu 2005, Chambers 2005, Liu et al. 2019). While we cannot directly infer the mechanisms through which wildfires alter microclimates because we did not fully characterize the surface energy budget, our results are consistent with studies documenting increased air temperature or VPD after fires (Ripley and Archibold 1999, Ma et al. 2010, Bello-Rodríguez et al. 2019), and studies that examined the influence of canopy cover on microclimate independent of fire (e.g., Davis et al. 2019*b*).

The differences in daily maximum temperature and VPD observed in this study are large enough to be biologically meaningful for understory plants and tree regeneration. Survival of tree seedlings in early life stages depends on environmental conditions near the ground surface (Johnson et al. 2011). High temperatures can directly girdle stems, and high evaporative potential (i.e., VPD) in the absence of ample soil water causes moisture stress and ultimately mortality (Kolb and Robberecht 1996, Johnson et al. 2011, Reinhardt et al. 2015). For example, an increase in mean midday air temperatures during the growing season of 3.2–4.4°C reduced seedling survival of *P. ponderosa* and *P. menziesii* by ~30–60% in an experimental study in Colorado (Rother et al. 2015). In the current study, we

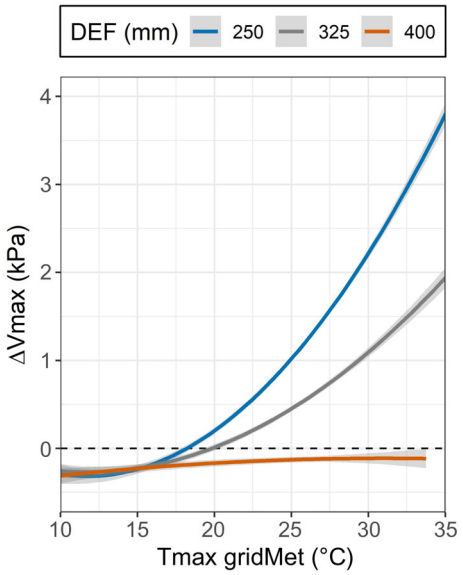

Fig. 5. Model predictions of ΔV_{max} after controlling for differences in canopy cover between paired burned and unburned sites, where higher ΔV_{max} values indicate higher VPD in the burned plot. Trends in ΔV_{max} are graphed against $T_{max}A$ for varying levels of DEF, where high DEF indicates lower moisture availability. Shaded bands show 95% confidence intervals for quadratic fits.

found that daily differences in maximum temperature and VPD between burned and unburned plots averaged 4.8 ± 4.5°C and 1.2 ± 1.3 kPa during the hottest 10 consecutive days of the study period, with maxima of 12.8°C and 4.7 kPa. Since our study was not designed to quantify the precise conditions experienced by seedlings, we can only make limited inferences into the biotic impacts of the observed changes. Nevertheless, fire-induced changes in microclimate of the magnitude documented clearly have the potential to impact the establishment and survival of tree seedlings and likely other understory vegetation (Stevens et al. 2015, Rother et al. 2015, Hansen and Turner 2019, Davis et al. 2019*a*).

Fire-related changes in microclimate vary with fire severity

While it is evident that wildfire affects postfire microclimate conditions, we found that these effects were not uniform across environmental and fire-severity gradients. Consistent with our hypotheses, warm-dry microclimate extremes were greatest among sites that experienced high-severity fire (Appendix S2: Fig. S2). This effect of fire severity on microclimate was due in part to canopy loss, as evidenced by our statistical models predicting differences in daily maximum temperature and VPD between paired burned and unburned plots. Fire-caused differences in microclimate were greater at sites that had larger differences in canopy cover (Fig. 3), consistent with studies that demonstrate the strong influence of canopy cover on microclimatic buffering capacity (e.g., Rambo and North 2009, Suggitt et al. 2011, von Arx et al. 2013, Davis et al. 2019*b*). After accounting for variability in total canopy cover, our final statistical models revealed no additional effect of variability in live vs. dead canopy cover among plots (represented by the Axis1 metric); this suggests that moderate- and high-severity fire most strongly affected microclimate directly through the loss of canopy shading. Residual dead trees, including the fine branches that are retained for several years after fire, can thus contribute significantly to regulating near-ground microclimates after fire (Fontaine et al. 2010, Hoecker et al. 2020), potentially increasing the likelihood of successful postfire tree regeneration where seed availability is not limiting.

In addition to the importance of canopy cover, our statistical models suggest that fire severity also affects microclimate through its impact on understory cover, which interacts with topography (i.e., solar exposure) to influence temperature extremes. Maximum temperatures tended to be higher at sites with more bare ground and less understory vegetation (Fig. 4). Several mechanisms likely account for this pattern. Understory plant transpiration may contribute to evaporative cooling, which was likely most important in severely burned areas where overstory transpiration was low. This effect was least pronounced in sites with high solar exposure, where midday temperatures are more likely to be driven by direct solar radiation, particularly if plants reduce stomatal conductance in response to moisture stress (Marshall and Waring 1984; Fig. 4). Further, albedo tends to increase with total vegetation cover after fire (Tsuyuzaki et al. 2009), suggesting that greater reflectance in sites with more understory vegetation regulated

temperature extremes. These results imply that microclimate extremes will attenuate over time as vegetation reestablishes, although the microclimatic buffering capacity of structurally complex stands may take decades to develop (Frey et al. 2016, Kovács et al. 2017, Bello-Rodríguez et al. 2019).

Fire-related changes in microclimate vary with biophysical context

The effect of wildfire on microclimate also depends strongly on biophysical context. We found that sites with high long-term climatic water availability experienced larger fire-caused changes in microclimate. The effect of water availability on microclimate is both direct, through evaporative cooling (i.e., latent heat flux), and indirect, through its influence on vegetation. Drier sites, with lower water availability to support evapotranspiration, have less potential to buffer microclimatic extremes independent of differences in canopy cover (Davis et al. 2019*b*). Sites with low long-term water availability also support less vegetation, consistent with a modest negative correlation between total basal area and climatic water deficit ($r = -0.47$; $P = 0.005$, $t = -3.0$, df = 31). Under canopies with low leaf area, the capacity for microclimatic buffering is low and declines as ambient conditions become warmer and drier (von Arx et al. 2013), perhaps due to greater direct solar radiation and turbulent air mixing. In contrast, in cool-mesic sites, conditions in burned areas became increasingly warm and dry relative to unburned forest as ambient temperatures increased, revealing greater relative impacts of fire on microclimate compared with warm-dry sites (Figs. 4, 5). Although we did not distinguish between the direct and indirect effects of local water balance on microclimate, our results indicate that moisture availability, and to a lesser extent solar exposure, govern the degree to which wildfires impact microclimate.

The remaining unexplained variability in temperature and VPD in our models likely reflects the lack of information on daily and seasonal changes in insolation or soil moisture, and fire effects on soil hydrology. Differences in canopy structure interact with soil water to influence understory microclimates (von Arx et al. 2013), and fire can result in either increased or decreased soil moisture (Certini 2005, Ma et al. 2010, Cardenas and Kanarek 2014). Further, soil moisture affects both microclimate conditions and the vulnerability of vegetation to changes in air temperature and VPD. Despite this caveat, our results suggest that the impacts of wildfires on microclimatic extremes increase with fire severity, decrease with vegetation regrowth, and are greatest in climatically cool-wet sites.

Implications for forest response to climate warming and increased wildfire activity

Altered microclimate in postfire environments is a key mechanism through which fire can catalyze vegetation changes that otherwise unfold more slowly with ongoing climate change. Microclimatic buffering mitigates the effects of climate change on understory organisms by reducing their exposure to climatic extremes (Jentsch and Beierkuhnlein 2008, De Boeck et al. 2011, Reyer et al. 2013). Empirical evidence highlights that plant–water relations are particularly sensitive to extremes in aridity (Reyer et al. 2013), implying that fire-induced losses of forest buffering capacity increase the vulnerability of understory plants to climatic stressors. Further, given strong linkages between VPD and fire activity in western North America (Sedano and Randerson 2014, Parks and Abatzoglou 2020, Higuera and Abatzoglou 2021), elevated VPD may increase the vulnerability of recently burned areas to subsequent fire if fuel is not limiting, which can ultimately erode forest resilience (Turner et al. 2019). While our results suggest that retention of standing dead trees and postfire vegetation recovery would attenuate the impacts of fire on microclimate, fire-induced changes in microclimate are nevertheless significant enough to impact patterns of plant regeneration. These impacts may be direct, by favoring species that are more drought-tolerant or species that are able to regenerate through resprouting (Davis et al. 2018), or indirect, by altering future patterns of burning.

Our results also suggest that we may be underestimating the potential impacts of fire-caused changes in microclimate in cool-moist settings. While fire-catalyzed vegetation shifts are considered most likely near the warm-dry edges of species ranges (e.g., Donato et al. 2016, Davis et al. 2019*a*), we found that cool-moist forests

experienced greater relative impacts of fire on microclimate due to differences in canopy cover and local water balance (Davis et al. 2019*b*). This suggests that fire-caused changes in microclimate could amplify regional warming, further pushing conditions closer to climatic limits for tree regeneration (Andrus et al. 2018, Davis et al. 2019*a*). Anticipating vegetation responses to the combined impacts of climate warming and increasing fire activity in cool-moist forests should thus take into account the substantial effects of fire on microclimate conditions.

Finally, our study informs management goals focused on maintaining forests for a host of ecosystem services. Our findings suggest that management actions aimed at reducing fire severity in low-elevation forests would help ameliorate postfire microclimate extremes, particularly in cooler and moister settings. This is consistent with the recognized importance of potential fire refugia that promote forest resilience through seed provision (Krawchuk et al. 2016, Coop et al. 2019). Similar efforts to reduce fire severity in cool-moist subalpine and mixed-conifer forests, while impactful on postfire microclimate, would have little ecological basis given a history of high-severity crown fire (e.g., Schoennagel et al. 2004). Further, our results imply that retaining standing dead trees after fires contributes to the moderation of microclimates and can thus indirectly support postfire tree regeneration.

The inferences from this study apply most directly to the biophysical context of mixed-conifer and subalpine forests of the northern Rocky Mountains, which represent a small range of conditions relative to forests of western North America. In addition, it remains uncertain how microclimate conditions will change over time after fire in cool-wet and warm-dry forest types, which differ in rates of vegetation recovery. Future research should examine these relationships over a wider range of climate and forest conditions (e.g., structure, fire severity), and over longer timescales, to better understand the interactive effects of fire, vegetation, and local water balance on microclimatic buffering.

Acknowledgments

We thank Z. Holden for sharing climate data, and A. Hendryx, M. Miller, R. Kirk-Davidoff, and S. Ammentorp for assistance with data collection and entry. We thank Kurt Wetzstein and the Lolo National Forest for cooperation with site selection and sampling, and Vince Archer for his insights on the study region. This work was supported by grants from the Joint Fire Science Program, through the Graduate Research Innovation program award 18-1-01-53 (KDW, PEH, KTD), and awards 16-1-01-15 (to PEH, KTD, and SZD) and 16–3-01–24 (to PEH).

Literature Cited

Abatzoglou, J. T. 2013. Development of gridded surface meteorological data for ecological applications and modelling. International Journal of Climatology 33:121–131.

Abatzoglou, J. T., and A. P. Williams. 2016. Impact of anthropogenic climate change on wildfire across western US forests. Proceedings of the National Academy of Sciences of the United States of America 113:11770–11775.

Anderson-Teixeira, K. J., A. D. Miller, J. E. Mohan, T. W. Hudiburg, B. D. Duval, and E. H. DeLucia. 2013. Altered dynamics of forest recovery under a changing climate. Global Change Biology 19 :2001–2021.

Andrus, R. A., B. J. Harvey, K. C. Rodman, S. J. Hart, and T. T. Veblen. 2018. Moisture availability limits subalpine tree establishment. Ecology 99:567–575.

Balch, J., T. Schoennagel, A. Williams, J. Abatzoglou, M. Cattau, N. Mietkiewicz, and L. St. Denis. 2018. Switching on the big burn of 2017. Fire 1:1-17.

Bello-Rodríguez, V., L. A. Gómez, Á. Fernández López, M. J. Del-Arco-Aguilar, R. Hernández-Hernández, B. Emerson, and J. M. González-Mancebo. 2019. Short- and long-term effects of fire in subtropical cloud forests on an oceanic island. Land Degradation & Development 30:448–458.

Brown, C. D., J. Liu, G. Yan, and J. F. Johnstone. 2015. Disentangling legacy effects from environmental filters of postfire assembly of boreal tree assemblages. Ecology 96:3023–3032.

Brown, D. J., I. Mali, and M. R. J. Forstner. 2014. Wildfire and Postfire restoration action effects on microclimate and seedling pine tree survivorship. Journal of Fish and Wildlife Management 5:174–182.

Cardenas, M. B., and M. R. Kanarek. 2014. Soil moisture variation and dynamics across a wildfire burn boundary in a loblolly pine (*Pinus taeda*) forest. Journal of Hydrology 519:490–502.

Certini, G. 2005. Effects of fire on properties of forest soils: a review. Oecologia 143:1–10.

Chambers, S. D. 2005. Fire effects on net radiation and energy partitioning: contrasting responses of

tundra and boreal forest ecosystems. Journal of Geophysical Research 110:D09106.

Coop, J. D., et al. 2020. Wildfire-driven forest conversion in western North American landscapes. BioScience 70:659–673.

Coop, J. D., T. J. Delory, W. M. Downing, S. L. Haire, M. A. Krawchuk, C. Miller, M. A. Parisien, and R. B. Walker. 2019. Contributions of fire refugia to resilient ponderosa pine and dry mixed-conifer forest landscapes. Ecosphere 10:e02809.

Crotteau, J. S., J. Morgan Varner, and M. W. Ritchie. 2013. Post-fire regeneration across a fire severity gradient in the southern Cascades. Forest Ecology and Management 287:103–112.

Davis, K. T., S. Z. Dobrowski, P. E. Higuera, Z. A. Holden, T. T. Veblen, M. T. Rother, S. A. Parks, A. Sala, and M. P. Maneta. 2019*a*. Wildfires and climate change push low-elevation forests across a critical climate threshold for tree regeneration. Proceedings of the National Academy of Sciences of the United States of America 116:6193–6198.

Davis, K. T., S. Z. Dobrowski, Z. A. Holden, P. E. Higuera, and J. T. Abatzoglou. 2019*b*. Microclimatic buffering in forests of the future: the role of local water balance. Ecography 42:1–11.

Davis, K. T., P. E. Higuera, and A. Sala. 2018. Anticipating fire-mediated impacts of climate change using a demographic framework. Functional Ecology 32:1729–1745.

De Boeck, H. J., F. E. Dreesen, I. A. Janssens, and I. Nijs. 2011. Whole-system responses of experimental plant communities to climate extremes imposed in different seasons. New Phytologist 189:806–817.

De Frenne, P., F. Zellweger, F. Rodríguez-Sánchez, B. R. Scheffers, K. Hylander, M. Luoto, M. Vellend, K. Verheyen, and J. Lenoir. 2019. Global buffering of temperatures under forest canopies. Nature Ecology & Evolution 3:744–749.

Donato, D. C., B. J. Harvey, and M. G. Turner. 2016. Regeneration of montane forests 24 years after the 1988 Yellowstone fires: A fire-catalyzed shift in lower treelines? Ecosphere 7:e01410.

Flannigan, M. D., K. A. Logan, B. D. Amiro, W. R. Skinner, and B. J. Stocks. 2005. Future area burned in Canada. Climatic Change 72:1–16.

Fontaine, J. B., D. C. Donato, J. L. Campbell, J. G. Martin, and B. E. Law. 2010. Effects of post-fire logging on forest surface air temperatures in the Siskiyou Mountains, Oregon, USA. Forestry 83:477–482.

Frey, S. J. K., A. S. Hadley, S. L. Johnson, M. Schulze, J. A. Jones, and M. G. Betts. 2016. Spatial models reveal the microclimatic buffering capacity of old-growth forests. Science Advances 2:e1501392.

Gillett, N. P., A. J. Weaver, F. W. Zwiers, and M. D. Flannigan. 2004. Detecting the effect of climate change on Canadian forest fires. Geophysical Research Letters 31:L18211.

Hansen, W. D., and M. G. Turner. 2019. Origins of abrupt change? Postfire subalpine conifer regeneration declines nonlinearly with warming and drying. Ecological Monographs 89:e01340.

Hesketh, M., D. F. Greene, and E. Pounden. 2009. Early establishment of conifer recruits in the northern Rocky Mountains as a function of postfire duff depth. Canadian Journal of Forest Research 39:2059–2064.

Higuera, P. E., and J. T. Abatzoglou. 2021. Record-setting climate enabled the extraordinary 2020 fire season in the western United States. Global Change Biology 27:1–2.

Hoecker, T. J., W. D. Hansen, and M. G. Turner. 2020. Topographic position amplifies consequences of short-interval stand-replacing fires on postfire tree establishment in subalpine conifer forests. Forest Ecology and Management 478:118523.

Holden, Z. A., A. E. Klene, R. F. Keefe, and G. G. Moisen. 2013. Design and evaluation of an inexpensive radiation shield for monitoring surface air temperatures. Agricultural and Forest Meteorology 180:281–286.

Holden, Z. A., A. Swanson, A. E. Klene, J. T. Abatzoglou, S. Z. Dobrowski, S. A. Cushman, J. Squires, G. G. Moisen, and J. W. Oyler. 2016. Development of high-resolution (250 m) historical daily gridded air temperature data using reanalysis and distributed sensor networks for the US Northern Rocky Mountains. International Journal of Climatology 36:3620–3632.

Holden, Z. A., A. Swanson, C. H. Luce, W. M. Jolly, M. Maneta, J. W. Oyler, D. A. Warren, R. Parsons, and D. Affleck. 2018. Decreasing fire season precipitation increased recent western US forest wildfire activity. Proceedings of the National Academy of Sciences of the United States of America 115: E8349–E8357.

Jentsch, A., and C. Beierkuhnlein. 2008. Research frontiers in climate change: effects of extreme meteorological events on ecosystems. Comptes Rendus - Geoscience 340:621–628.

Johnson, D. M., K. A. McCulloh, and K. Reinhardt. 2011. The Earliest Stages of Tree Growth: development, Physiology and Impacts of Microclimate. Pages 65–87 *in* F. C. Meinzer, B. Lachenbruch, and T. E. Dawson, editors. Size- and age-related changes in tree structure and function. Springer Netherlands, Dordrecht, The Netherlands.

Kemp, K. B., P. E. Higuera, P. Morgan, and J. T. Abatzoglou. 2019. Climate will increasingly determine post-fire tree regeneration success in low-elevation forests, Northern Rockies, USA. Ecosphere 10:e02568.

Kolb, P. F., and R. Robberecht. 1996. High temperature and drought stress effects on survival of Pinus ponderosa seedlings. Tree Physiology 16:665–672.

Kovács, B., F. Tinya, and P. Ódor. 2017. Stand structural drivers of microclimate in mature temperate mixed forests. Agricultural and Forest Meteorology 234–235:11–21.

Krawchuk, M. A., S. L. Haire, J. Coop, M. A. Parisien, E. Whitman, G. Chong, and C. Miller. 2016. Topographic and fire weather controls of fire refugia in forested ecosystems of northwestern North America. Ecosphere 7:e01632.

Kuznetsova, A., P. B. Brockhoff, and R. H. B. Christensen. 2017. lmerTest package: tests in linear mixed effects models. Journal of Statistical Software 82:1–26.

Liu, H. 2005. Changes in the surface energy budget after fire in boreal ecosystems of interior Alaska: an annual perspective. Journal of Geophysical Research 110:D13101.

Liu, Z., A. P. Ballantyne, and L. A. Cooper. 2019. Biophysical feedback of global forest fires on surface temperature. Nature Communications 10:214.

Ma, S., A. Concilio, B. Oakley, M. North, and J. Chen. 2010. Spatial variability in microclimate in a mixed-conifer forest before and after thinning and burning treatments. Forest Ecology and Management 259:904–915.

Marshall, J. D., and R. H. Waring. 1984. Conifers and broadleaf species: Stomatal sensitivity differs in western Oregon. Canadian Journal of Forest Research 14:905–908.

McCune, B., and D. Keon. 2002. Equations for potential annual direct incident radiation and heat load. Journal of Vegetation Science 13:603–606.

McKenzie, D., and J. S. Littell. 2017. Climate change and the eco-hydrology of fire: Will area burned increase in a warming western USA. Ecological Applications 27:26–36.

Monteith, J., and M. Unsworth. 2013. Principles of Environmental Physics: plants, Animals, and the Atmosphere. Page Principles of Environmental Physics: plants, Animals, and the Atmosphere. Fourth Edition. Elsevier Academic Press, Cambridge, Massachusetts, USA.

Montes-Helu, M. C., T. Kolb, S. Dore, B. Sullivan, S. C. Hart, G. Koch, and B. A. Hungate. 2009. Persistent effects of fire-induced vegetation change on energy partitioning and evapotranspiration in ponderosa pine forests. Agricultural and Forest Meteorology 149:491–500.

MTBS Project (USDA Forest Service/U.S. Geological Survey). 2019. MTBS Data Access: fire Level Geospatial Data. http://mtbs.gov

Parks, S. A., and J. T. Abatzoglou. 2020. Warmer and drier fire seasons contribute to increases in area burned at high severity in western US Forests From 1985 to 2017. Geophysical Research Letters 47: e2020GL089858.

PRISM Climate Group (Oregon State University). 2015. PRISM 30-Year Normals. Oregon State University. http://prism.oregonstate.edu

Rambo, T. R., and M. P. North. 2009. Canopy microclimate response to pattern and density of thinning in a Sierra Nevada forest. Forest Ecology and Management 257:435–442.

Refsland, T., and J. Fraterrigo. 2018. Fire increases drought vulnerability of *Quercus alba* juveniles by altering forest microclimate and nitrogen availability. Functional Ecology 32:2298–2309.

Reinhardt, K., M. J. Germino, L. M. Kueppers, J.-C. Domec, and J. Mitton. 2015. Linking carbon and water relations to drought-induced mortality in *Pinus flexilis* seedlings. Tree Physiology 35:771–782.

Reyer, C. P. O., et al. 2013. A plant's perspective of extremes: terrestrial plant responses to changing climatic variability. Global Change Biology 19:75–89.

Ripley, E. A., and O. W. Archibold. 1999. Effects of burning on prairie aspen grove microclimate. Agriculture, Ecosystems and Environment 72:227–237.

Rother, M. T., T. T. Veblen, and L. G. Furman. 2015. A field experiment informs expected patterns of conifer regeneration after disturbance under changing climate conditions. Canadian Journal of Forest Research 45:1607–1616.

Schoennagel, T., T. T. Veblen, and W. H. Romme. 2004. The interaction of fire, fuels, and climate across Rocky Mountain Forests. BioScience 54:661–676.

Sedano, F., and J. T. Randerson. 2014. Multi-scale influence of vapor pressure deficit on fire ignition and spread in boreal forest ecosystems. Biogeosciences 11:3739–3755.

Serra-Diaz, J. M., C. Maxwell, M. S. Lucash, R. M. Scheller, D. M. Laflower, A. D. Miller, A. J. Tepley, H. E. Epstein, K. J. Anderson-Teixeira, and J. R. Thompson. 2018. Disequilibrium of fire-prone forests sets the stage for a rapid decline in conifer dominance during the 21st century. Scientific Reports 8:6749.

Stevens, J. T., H. D. Safford, S. Harrison, and A. M. Latimer. 2015. Forest disturbance accelerates thermophilization of understory plant communities. Journal of Ecology 103:1253–1263.

Suggitt, A. J., P. K. Gillingham, J. K. Hill, B. Huntley, W. E. Kunin, D. B. Roy, and C. D. Thomas. 2011. Habitat microclimates drive fine-scale variation in extreme temperatures. Oikos 120:1–8.

Tsuyuzaki, S., K. Kushida, and Y. Kodama. 2009. Recovery of surface albedo and plant cover after wildfire in a *Picea mariana* forest in interior Alaska. Climatic Change 93:517–525.

Turner, M. G., K. H. Braziunas, W. D. Hansen, and B. J. Harvey. 2019. Short-interval severe fire erodes the resilience of subalpine lodgepole pine forests. Proceedings of the National Academy of Sciences of the United States of America 116:11319–11328.

von Arx, G., E. Graf Pannatier, A. Thimonier, and M. Rebetez. 2013. Microclimate in forests with varying leaf area index and soil moisture: potential implications for seedling establishment in a changing climate. Journal of Ecology 101:1201–1213.

Westerling, A. L. 2016. Increasing western US forest wildfire activity: sensitivity to changes in the timing of spring. Philosophical Transactions of the Royal Society of London. Series B, Biological Sciences 371:20150178.

Westerling, A. L., M. G. Turner, E. A. H. Smithwick, W. H. Romme, and M. G. Ryan. 2011. Continued warming could transform Greater Yellowstone fire regimes by mid-21st century. Proceedings of the National Academy of Sciences of the United States of America 108:13165–13170.

Young, A. M., P. E. Higuera, P. A. Duffy, and F. S. Hu. 2017. Climatic thresholds shape northern high-latitude fire regimes and imply vulnerability to future climate change. Ecography 40:606–617.

Data Availability

Data and code used in this study are available via the Dryad Data Repository: https://doi.org/10.5061/dryad.47d7wm3c6.

Supporting Information

Additional Supporting Information may be found online at: http://onlinelibrary.wiley.com/doi/10.1002/ecs2.3467/full